Structural insight into inositol monophosphate

Lucas Kraft, S. Mark Roe, Raj Gill, and John Atack

From the Sussex Drug Discovery Centre (SDDC), School of Life Sciences, University of Sussex, Brighton, UK

Running title: *Structural insight into IMPase*

To whom correspondence should be addressed: Prof. John Atack, Sussex Drug Discovery Centre, University of Sussex, Chichester II, Falmer, Brighton, BN1 9QJ, Telephone: +44 1273 872722; E-mail: J.Atack@sussex.ac.uk

Keywords: inositol monophosphate, IMPase, bipolar disorder, L-690,330, lithium, catalytic mechanism, co-crystallization

ABSTRACT

Lithium, still the gold standard in the treatment of bipolar disorder has been proposed to inhibit inositol monophosphatase (IMPase) and is hypothesized to exert its therapeutic effects by attenuating phopshatidylinositol (PI) cell signalling. Drug discovery efforts focused on small molecule lithium mimetics that specifically inhibit IMPase and therefore would not exhibit lithium's undesired side effects. One very potent and specific IMPase inhibitor is L-690,330. L690,330 was developed by Merck Sharp & Dome and is a competitive substrate-based inhibitor. We were interested in determining the exact binding mechanism of L-690,330 to make path for future structure-based drug discovery approaches. We firstly report here the X-ray crystallographic structure of IMPase in complex with L690,330. Additionally, we co-crystallized IMPase with its substrate Ins1P and observe movement of a mobile loop that was yet not reported.

Bipolar disorder is a disabling mental illness that is characterized by episodes of both elevated or irritable mood (hypomania or mania) and decreased energy and activity (depression) (1–3). It is estimated to have an overall lifetime prevalence of 2.4 % (4) and causes annual costs to societies in the range of billions (5, 6). Lithium still remains after six decades of usage (7) the first line choice for the treatment, prevention and prophylaxis of bipolar disorder, as it shows reduced relapses of both manic and depressive phases (8, 9) and is also the only known agent that reduces the suicide risk of patients (10, 11). Unfortunately, lithium has a problematic side effect profile. Lithium's very narrow therapeutic window (0.5 – 0.8 mmol/l) makes overdosing and intoxication easy and side effects even at proper usage can be severe. Side effects include nausea, diarrhea, tremor, weight gain, thyroid enlargement, diabetes insipidus and renal failure (12–18).

Lithium's mechanism of action still remains elusive. Lithium is a small cation that non-specifically interacts with many different targets, such as ion channels, enzymes and transporters and influences signalling cascades and neurotransmission (19). With such a range of actions, it has proved difficult (to impossible) to define lithium's mechanism of action and which interactions are responsible for its therapeutic effects as well its side effects. The lithium ion (Li^+) has a similar

hydrated radius to the magnesium ion (Mg^{2+}) and has therefore the ability to compete with magnesium (20, 21). Magnesium is an important cofactor for many enzymes and a few magnesium-dependent enzymes that are inhibited by lithium at therapeutic concentrations (0.6 – 1 mM) are documented. One of these enzymes is inositol monophosphatase (IMPase) (22).

IMPase (EC 3.1.3.25) is a highly conserved enzyme that hydrolyses inositol monophosphate to free inositol and phosphate in the phosphatidylinositol (PI) signalling cascade (23). The PI pathway is primarily activated by G proteins ($G_{i/o}$, G_q) that increase phospholipase C (PLC) activity. PLC hydrolyses phosphatidylinositol 4,5-bisphosphate (PIP_2) to inositol 1,4,5-trisphosphate (IP_3) and diacylgylcerol (DAG). Binding of IP_3 to the IP_3-receptor (IP_3-R) releases intracellular stored calcium into the cytoplasm, while DAG activates protein kinase C (PKC). Moreover, IP_3 is converted by different kinases and phosphatases to a variety of inositol phosphates that are involved in intracellular signalling. PIP_2 is regained mainly by recycling of IP_3. Different phosphatases sequentially dephosphorylate IP_3 to free inositol that is then reused by different enzymes to generate phosphatidylinositol (PI), phosphatidylinositol phosphate (PIP) and PIP_2 (24–27). IMPase is the last and rate-limiting phosphatase in the recycling of PIP_2 and hence is a crucial enzyme in the PI cycle. Inhibition of IMPase by lithium led to Berridge's "Inositol Depletion Hypothesis" in which attenuation of PI signalling is a result of inositol depletion and in turn leads to impaired PI recycling and production (28).

IMPase therefore remains an interesting therapeutic target for bipolar disorder. Great effort in finding and developing small molecule IMPase inhibitors was made in the 1990s by Merck Sharp & Dohme who synthesized potent substrate based inhibitors such as L-690,330 and L-693,369 (29). Unfortunately, most of these compounds showed low bioavailability (30). Nevertheless, the esterified prodrug L-690,488 had favourable penetrability and mimicked lithium's effect on the PI pathway in human cell lines (30). Additionally, intracerebroventricular administration of L-690,330 to mice in form of liposomes ameliorated pilocarpine induced behaviour and their behaviour in the forced swim test similar to mice treated with lithium (31). With increasing advancement in drug delivery systems, these potent and specific inhibitors may gain new interest in the treatment of bipolar disorder.

Surprisingly, no structure-based approach was used to date to determine the exact binding mechanism of these inhibitors. Crystal structures in complex with one of these inhibitors would shed light on their exact binding mechanism and may provide valuable insight for their improvement in potency and bioavailability. Here, we firstly report the X-ray crystallographic structure of human IMPase in complex with the potent antagonist L-690,330. Moreover, we resolved the structure in complex with inositol 1-phosphate (Ins1P) and observe movement of a mobile loop that was yet not reported and that provides strong insight into IMPase catalytic mechanism.

RESULTS

L-690,330 strongly increases thermal stability of IMPase – The potent antagonist L-690,330 was designed based on the substrate Ins1P. Baker *et al* (32, 33) showed that the hydroxyl groups at positions 2 or 6 and 4 are important for substrate binding to the enzyme while the other hydroxylgroups are not. Based on these findings, different inhibitors were synthesized that include a phenolic bisphosphonate series with L-690,330 having one of the highest affinities to IMPase (29). To confirm its affinity with published data, the inhibitory effect of L-690,330 on IMPase was

tested using the malachite green assay for phosphate detection. Its biochemical characterization revealed an inhibitory concentration (IC_{50}) of 0.22 ± 0.01 µM (Fig. 1*B*) which is in accordance with the literature (34).

Binding of L-690,330 was further investigated by differential scanning fluorimetry (DSF). At high temperatures most proteins destabilize, unfold and expose hydrophobic residues. This unfolding is monitored in DSF through dyes that bind and fluoresce in non-polar environments and the melting point T_m of a protein can be calculated. Small molecules that bind to the protein often stabilize it and shift the melting point to higher temperatures (35). IMPase on its own has a remarkable melting point of 79°C (Fig. 1*B*). This explains why heat treatment during the purification process is possible as recommended by McAllister *et al* (36) without denaturing or precipitating the protein. Addition of L-690,330 to the reaction mixture reveals concentration dependent stabilization of IMPase by the inhibitor. At high concentrations, the protein melting point is shifted by up to 15 °C. In fact, at inhibitor concentrations of 30 µM, the melting curve cannot be fully visualized (Fig. 1*A*).

2-(N-morpholino)ethanolsulfonic acid binds to the active site – To compare the structural mechanism on how L-690,330 inhibits IMPase function, we aimed to obtain three crystal structures: one structure just in complex with its metal cofactors, one in complex with the substrate Ins1P and one in complex with L-690,330. Primarily crystallization attempts indicated that IMPase preferably crystallizes in the presence of divalent salts (e.g. magnesium, calcium or manganese salts), a Good buffer (e.g. MES, Bis Tris propane, Tris HCl) and polyethylene glycol (PEG) 3350 or 4000. By testing different combinations of salt, buffer and PEG, a combination of $MnSO_4$ or $CaCl_2$, MES at pH 5.5 and PEG 4000 turned out to be the most promising condition in crystallizing IMPase and yielded large and well diffracting crystals.

Surprisingly, we observed electron density for 2-(*N*-morpholino)ethanolsulfonic acid (MES) in the active site of IMPase while resolving the enzyme's structure that was aimed to be just with its metal cofactors. The crystal with MES diffracted to 1.79 Å resolution (Tab. 1) and contains two molecules in its asymmetric unit. Both molecules assemble as homodimers and show the αβαβα core structure that is characteristic for IMPase (37). Each monomer holds three manganese ions, a MES molecule and a glycerol in its large and hydrophilic active site (Fig. 2). Structural comparison and superposition with the published structure 4AS4 (38) yielded a root-mean-square-deviation of atomic positions (RMSD) of 0.407 Å and shows identical location of all metal ions, as well as identical orientation of residues that form the pocket. Thus, binding of MES seems not to alter the shape of the active site or induce movement of specific residues. In accordance, activity of IMPase in the malachite green assay is not affected by MES (data not shown).

Crystallization with calcium induces movement of a mobile loop – Co-crystallization of IMPase with its substrate required calcium as salt. Calcium inhibits hydrolytic activity of IMPase (22) and therefore makes co-crystallization with Ins1P feasible. Crystals with Ins1P only grew when using crystal micro seeds that were obtained from previous crystals grown in the presence of calcium. Successfully grown crystal diffracted to 2.01 Å resolution (Tab. 1) and has four identical molecules in one cell unit. Each molecule holds one Ins1P molecule in the active site and up to three calcium ions (three in chain A, two in chain B, C and D). Only in chain A electron density is clear for all residues. As for the other chains, certain regions are disordered and could not be modelled. These regions include residues 28-43 and 73-78 in chain B, 35-37 in chain C and 30-43, as well as 70-79 in chain D.

Interestingly, the loop from residues 28-43 that forms part of the active site seems to affect binding of the third calcium ion and thus, the third calcium ion cannot be observed in chain B, C and D (Fig. 3).

Structural alignment (chain A and B) with the structure in complex with MES shows high similarity (RMSD 0.693 Å) but strikingly reveals different orientation of residues 28-43. This mobile loop moves away from the active site in the crystal structure with Ins1P. More specifically, Lys36 is pointing away and no longer interacts with other residues that form the pocket (Fig. 4*B*). In the structure co-crystallized with MES and manganese, Lys36 interacts with Glu71 via a salt bridge (Fig. 4*A*).

The substrate interacts with various residues in the active site (Fig. 5*A*). The inositol ring is mainly held by hydrogen bonds that are formed in between Glu213 and O4, as well as Asp93 and O2 of the sugar ring. Metal ion contacts are exclusively formed between the calcium ions and the oxygens of the phosphoryl group. Detailed and solvent including interactions are shown in figure 5*A*. Protein alignment of both resolved structures reveals different orientation of the MES sulfonate group and the substrate's phosphoryl group. Interestingly, the glycerol in the structure resolved with MES and manganese seems to mimic the inositol ring (Fig. 5*B*). Residues that are involved in substrate binding however show identical conformation in both structures.

L-690,330 is stabilized by additional residues in the pocket – Initial attempts to co-crystallize IMPase with L-690,330 failed because DMSO, in which L-690,330 was dissolved, strongly influenced crystal growth and only low-quality crystals were obtained. Therefore a similar approach as in the previous substrate co-crystallization experiment was tested by dissolving the inhibitor in the buffer IMPase is stored in. Due to the strong hydrophilic properties of L-690,330 dissolving in storage buffer was easy and co-crystallization experiments with this stock solution yielded well diffracting crystals.

The crystal diffracted to 1.39 Å resolution (Tab. 1) which is the best resolution of human IMPase obtained to date. No significant secondary structure differences are found when comparing to the structure with MES. The mobile loops that were partly disordered in the structure crystalized in the presence of calcium and the substrate are ordered and Lys36 is pointing towards the pocket. Each chain holds three manganese ions, one L-690,330 molecule, as well as several glycerol. Interaction of L-690,330 with the protein backbone is similar to the substrate. One key interaction is the hydrogen bond between the para oxygen of the ligand to the carboxylate group of Glu213. All three manganese ions interact with the phosphonate groups of the inhibitor and the extra phosphoryl group of L-690,330 interacts with additional residues Trp219 and Asp220 which is likely to contribute to the strong binding of the inhibitor to the pocket (Fig. 6).

DISCUSSION

Other crystallographic studies observed up to three magnesium or manganese binding sites in human IMPase (38, 39), however, no studies reported binding of MES buffer to date. Also binding of MES does not seem to be strong (it is easily outcompeted by lower concentrations of inositol 1-phsophate and L-690,330 in the other crystallization conditions) and does not affect the enzyme's catalytic activity, here resolved structure underlines that IMPase's active site is very large (larger than necessary to accommodate the substrate). This makes it possible for IMPase to hydrolyse a variety of other substrates (40–43). Interestingly, the MES molecule does not orientate like the substrate or substrate mimetic L-690,330 in the active site but instead fills in other parts of the pocket. This observation could potentially be utilized to design novel IMPase inhibitors that do not mimic the

substrate but instead take advantage of the large pocket and bind to different residues.

The crystal structures of IMPase in complex with Ins1P and the substrate mimetic L-690,330 give invaluable insight into IMPase catalytic function. Especially the structure co-crystallized with Ins1P and calcium and its unique structural features that are not reported in any other published structure to date. The mobile loop that is formed by residues 28-43 and that is only observed in chain A of the crystal structure takes in an "open" conformation with Lys36 pointing away from the pocket. Movement of Lys36 is interesting in this regard as it seems to be involved in the catalytic mechanism of IMPase. Mutagenic studies by Ganzhorn *et al.* (44) in which Lys36 was mutated to Gln36 showed a decrease in IMPase's turnover of the substrate. Suggestive is that Lys36 increases the polarizing effect of one of the metal ions by interacting with Glu70 or Glu71. This would decrease the negative charge of the glutamate residues to which the magnesium ion is exposed and thus would induce hydrolysis of the substrate (44). Different conformations of the mobile loop were also observed in the homologue of *Archaeoglobus fulgidus*. It was proposed that the mobility of this loop is associated with metal and/ or substrate binding and is important for product release (45). Identical role in the human form should not be excluded.

Other structures in complex with Ins1P are described. 1IMA and 1IMB were co-crystallized with D-*myo*-Ins1P and gadolinium and L-*myo*-Ins1P and gadolinium respectively (46). Moreover, Ganzhorn *et al.* (47) deposited IMPase in complex with the substrate and calcium (1AWB). Structural alignment of here resolved structure with 1AWB reveals same orientation of all calcium ions, as well as the substrate, however, Lys36 points towards the active site in the deposited structure. This observation was surprising to us as we hypothesized that calcium somehow exerts its influence on the mobile loop that ultimately leads to its distinct conformation. As calcium is found in the active site of 1AWB it must also be for other reason than calcium that Lys36 points away in here resolved structure. Any influence of the crystal symmetry should not be disregarded. It remains unclear why the mobile loop did not crystalize identical to published structures such as in 1AWB or 4AS4 and is rather disordered in certain chains instead of taking in energetically favourable conformation (i.e. Lys36 towards the active site). Nevertheless, here resolved crystal structure provides a "snapshot" of its movement that can explain on how calcium may exert its inhibitory effect on IMPase.

Lastly, IMPase in complex with L-690,330 is described with the highest resolution available to date. Superimposition with the structure in complex with MES revealed no structural differences in between the pockets and alignment with the structure co-crystallized with the substrate emphasizes that L-690,330 mimics the substrate. As L-690,330 is essentially a non-hydrolysable substrate, the crystal structure in complex with this inhibitor confirms that the mobile loop containing Lys36 orientates towards the active site when binding the substrate and activating manganese.

Our structural findings strongly suggest movement of the mobile loop in the course of catalysis. As observed by Ganzhorn *et al.* (44), two segments of the active site appear to undergo structural changes upon substrate and metal binding. These segments comprise residues 30-40 and 70-75. The latter segment was observed to be partly disordered in the structure here crystallized with Ins1P and was previously shown to move away from the cation binding site in the apo enzyme structure (39). These two segments might approach each other for catalysis and Lys36 through salt bridge interactions with Glu70 and/or Glu71 would facilitate their approach.

EXPERIMENTAL PROCEDURES

Materials – All materials were purchased from Sigma-Aldrich or Fisher Scientific and were the highest purity available if not stated otherwise. Ampicillin was purchased from Melford and L-690,330 from Tocris Bioscience.

Preparation of human recombinant IMPase – Human cDNA for full length IMPase with an amino terminal 6 histidine tag and 3C protease cleavage site was synthesized and subcloned into a pET15b vector by GenScript®. Expression of recombinant human IMPase was described elsewhere (38). Hence, transformed *Escherichia Coli* Rosetta2(DE3) cells (Merck Millipore) were grown in Luria-Bertani (LB) broth containing 50 µg/mL ampicillin and 35 µg/mL chloramphenicol overnight at 37°C and 200 rev min^{-1}. Cells from this culture were used to inoculate LB broth containing 2.5 mM betaine, 660 mM sorbitol, 50 µg/mL ampicillin and 35 µg/mL chloramphenicol and grown at 37°C until the OD_{600} reached 0.2-0.3. The temperature was decreased to 25°C and cells further incubated until the OD_{600} reached 0.6. Protein expression was induced by the addition of 0.4 mM isopropyl-β-*D*-thiogalactopyranoside (IPTG) and the culture was left overnight at 180 rev min^{-1} and 25°C. Bacterial cells were harvested by centrifugation at 9600 x *g* for 20 min at 4°C and resuspended lysis buffer (20 mM Tris-HCl pH 7.8, 150 mM NaCl, 40 U/mL DNAse I (Sigma-Aldrich) and 1 EDTA-free protease inhibitor tablet (Thermo Scientific) per 50 mL). The pellet was lysed by ultrasonication and the soluble protein separated by centrifugation at 33000 x *g* for 20 min at 4°C. The supernatant was heat treated at 68°C for 1 h and the precipitated protein was pelleted by centrifugation at 32816 x *g* for 20 min at 4°C. The supernatant was then incubated at 4°C for 1 h with TALON superflow resin (GE Healthcare) that was pre-equilibrated with binding buffer (20 mM Tris-HCl pH 7.8, 150 mM NaCl, 10 mM imidazole). After incubation, the resin was washed with wash buffer (20 mM Tris-HCl pH 7.8, 150 mM NaCl, 15 mM imidazole) and the protein eluted with elution buffer (20 mM Tris-HCl pH 7.8, 150 mM NaCl, 250 mM imidazole). Elution fractions were pooled and the 6 histidine tag cleaved overnight at 4°C by the addition of PreScission protease (see below) at a protease-to-protein ratio 1:100 (w/w). After digestion, PreScission protease was separated from the target protein by incubating the digestion mixture with Glutathione Fast 4 flow resin (GE Healthcare) that was pre-equilibrated with size exclusion chromatography (SEC) buffer (20 mM Tris-HCl pH 7.8, 150 mM NaCl). The collected flow through was concentrated to approximately 5 mL using viva spin concentrators (Sartorius Stedim) at 4000 x *g* and 4°C and applied on a with SEC buffer equilibrated gel filtration column (HiLoad 16/600 Superdex 75 prep grade, GE Healthcare) using the ÄKTA FPLC system from GE Healthcare. Protein was eluted at a flow rate of 2.5 mL/min and fractions analysed by SDS PAGE using NuPAGE® Novex® 4-12% Bis-Tris protein gels (life technologies). Fractions containing the protein were pooled, concentrated and re-buffered into storage buffer (20 mM Tris-HCl pH 7.8, 150 mM NaCl, 1 mM EDTA, 10 % glycerol (v/v)) using viva spin concentrators at 4000 x *g* and 4°C.

Preparation of PreScission protease – Glutathione S-transferase (GST) tagged HRV 3C protease (PreScission protease) cloned into a pGEX-1 vector was used to transform Rosetta2(DE3) cells. Transformed cells were used to inoculate a pre-culture of LB broth supplemented with 50 µg/mL ampicillin and 35 µg/mL chloramphenicol and grown overnight at 37°C and 200 rev min^{-1}. Cells were used the next day to inoculate the main culture using the same broth and antibiotics and grown at 180 rev min^{-1} until reaching an OD_{600} of approximately 0.6. Flasks were put on ice for 15 min, induced with 0.2 mM IPTG and grown

overnight at 20°C and 180 rev min^{-1}. The next day, cells were harvested by centrifugation at 9600 x *g* for 20 min at 4°C and resuspended lysis buffer (50 mM Tris-HCl pH 8.0, 1000 mM NaCl, 1 mM EDTA, 1 mM DTT) and lysed by ultrasonication. Soluble protein was separated by centrifugation at 33000 x *g* for 20 min at 4°C and the supernatant applied on a with lysis buffer pre-equilibrated GST Trap FF column (GE Healthcare). The column was extensively washed with lysis buffer and protein eluted with 10 mM reduced glutathione in lysis buffer. Fractions were analysed by SDS PAGE as described above and protein containing fractions pooled and dialyzed overnight into storage buffer (50 mM Tris-HCl pH 8.0, 150 mM NaCl, 10 mM EDTA, 1 mM DTT, 20 % (v/v) glycerol).

Malachite green assay and DSF – The inhibitory effect of L-690,330 was tested using the malachite green assay (48–50). A 10-point dose response curve was recorded to determine L-690,330's inhibitory concentration (IC_{50}). For this, L-690,330 (30 µM highest concentration) was added to 0.08 ng/µL IMPase in assay buffer (50 mM Tris-HCl pH 7.4, 3 mM $MgCl_2$, 150 mM KCl, 0.5 mg/mL bovine serum albumin (BSA), 0.01 % (w/v) Triton X-100) and incubated at room temperature for 10 min. Then, 0.075 mM inositol 1-phosphate was added, incubated at 37°C for 30 min and the reaction stopped and phosphate formation detected by adding BIOMOL GREEN solution (Enzo life science). The plate was incubated at room temperature for 30 min and the absorbance then measured at λ= 630 nm on the PHERAstar FS plate reader (BMG labtech). Data was analyzed and plotted with PRISM 7.0.2 (GraphPad).

To determine the melting points of IMPase in the presence of L-690,330, the inhibitor (30 µM highest concentration) was mixed with 6 µM IMPase in DSF assay buffer (50 mM HEPES pH 7.4, 3 mM $MgCl_2$, 150 mM KCl, 1 mM EGTA) and incubated at room temperature for 10 min. Then 4 x SYPRO Orange dye (Sigma-Aldrich) was added and melting curves were recorded on the LightCylcer 480 II (Roche). To determine the enzyme's melting point on its own, IMPase at different concentrations in DSF buffer was mixed with 4 x SYPRO Orange dye and the melting curve directly recorded. Integration time was set manually to 1 sec. The temperature was hold at 20°C for 1 min and then increased by 1°C every 0.4 min up to a maximal temperature of 95°C. Data was integrated and analysed using the LightCycler 480 SW 1.5 program (Roche); melting points were determined manually.

Crystallization – Crystallization of human IMPase was carried out on VDX plates (Hampton research) using the hanging drop method or 2 well MRC plates (Swissci) using the sitting drop method.

To crystallize human IMPase in the presence of manganese, equal volumes (1 µL) of the target protein in storage buffer (20 mg/mL) and reservoir solution (0.12 M $MnSO_4$, 0.1 M MES pH 5.5, 24 % (w/v) PEG 4000) were mixed and incubated at room temperature for a few days.

Human IMPase in complex with the potent inhibitor L-690,330 was crystallized at room temperature using the hanging-drop method and micro seeding. Seeds were obtained from crystals described above using the Seed Bead kit from Hampton research. Human IMPase in storage buffer (20 mg/mL) was firstly incubated at 37°C for 15 min in the presence of 5 mM L-690,330 that was previously dissolved in storage buffer. Then, equal volumes (1 µL) of the enzyme-inhibitor mix and reservoir solution (0.2 M $MnSO_4$, 0.1 M MES pH 5.5, 25 % (w/v) PEG 4000) containing seeds (diluted 1:100 in reservoir solution) were mixed and incubated at room temperature for a few days.

Human IMPase in complex with the substrate was crystallized at room temperature using the sitting-drop method and micro seeding. Seeds were obtained from crystals

grown in the presence of $CaCl_2$. For this, equal volumes (1 µL) of human IMPase in storage buffer (20 mg/mL) and reservoir solution (0.2 M $CaCl_2$, 0.1 M MES pH 5.5, 25 % (w/v) PEG 4000) were mixed and incubated at room temperature for a few days. Formed crystals were used to produce crystal micro seeds using the Seed Bead kit from Hampton research. To co-crystallize human IMPase with inositol 1-phosphate, human IMPase in storage buffer (20 mg/mL) was incubated at 37°C for 8 min in the presence of the substrate (8 mM, dissolved in water). Then, equal volumes (1 µL) of the enzyme-substrate mix and reservoir solution (0.2 M $CaCl_2$, 0.1 M MES pH 5.5, 25 % (w/v) PEG 4000) containing seeds (diluted 1:100 in reservoir solution) were mixed and incubated at room temperature for a few days.

All crystals were transferred from 0 to 30 % (v/v) glycerol in steps of 10 % prior to flash cooling in liquid nitrogen and data collection. X-ray diffraction data was collected at the Diamond Light Source (Oxfordshire, United Kingdom) on the I04 beamline (λ = 0.9795 Å) using a Dectris Pilatus 6M-F detector. The crystals were cooled at 100 K during data collection by a Cryostream (Oxford Cryosystems Ltd). Data were integrated and scaled using the automatic Xia2 processing at the Diamond Light Source.

Part of the structures were initially solved by molecular replacement using previously determined structures. For the structure with manganese and MES in the active site a published structure of human IMPase (PDB 4AS4) was used in the usual spacegroups (P 32 2 1). For the structure in complex with L-690,330, the refined structure with manganese and MES in the active site was used as a model. For the structure in complex with inositol 1-phosphate, a structure that was crystallized in the presence of calcium in our laboratories was used as a model (not disclosed).

Data was processed with CCP4 (51), Phenix (52) and Buster (53) and manual rebuilding was performed in Coot (54). All pictures and operations were conducted in Maestro version 10.6 (Schrödinger). Before analysis, protein structures were prepared using Maestro's integrated protein preparation wizard: Bond orders were assigned, hydrogens were added, zero-order bonds to metals and disulfide bonds were created, as well as water beyond 5 Å from hetero groups were deleted. Moreover, the protein was refined by assigning hydrogen bonds at pH 7.0. Interaction diagrams were manually plotted with ChemDraw Prime 15.1 (PerkinElmer).

Acknowledgments: We thank Dr Trevor Askwith for assistance on the malachite green assay and Dr. Ben Wahab for assistance on the Maestro (Schrodinger) suite. We also acknowledge Dr. Antony Oliver for providing the plasmids for the expression of human IMPase and PreScission protease and Dr. Nasrin Jahan on assisting during purification, as well as setting up crystal plates. Lastly, we thank Gareth Williams for helping with the DSF experiments.

Conflict of interest: The authors declare they have no conflicts of interest with the contents of this article.

Author contribution: LK conducted most of the experiments, analysed the results and wrote most of the paper. MR collected crystal data at the diamond light source. JA conceived the idea for the project and wrote the paper with LK.

REFERENCES

1. WHO (2010) ICD-10, Bipolar affective disorder
2. National Institute of Mental Health NIH - Bipolar disorder
3. Müller-Oerlinghausen, B., Berghöfer, A., and Bauer, M. (2002) Bipolar disorder. *Lancet (London, England)*. **359**, 241–7
4. Merikangas, K. R., Jin, R., He, J.-P., Kessler, R. C., Lee, S., Sampson, N. A., Viana, M. C., Andrade, L. H., Hu, C., Karam, E. G., Ladea, M., Medina-Mora, M. E., Ono, Y., Posada-Villa, J., Sagar, R., Wells, J. E., and Zarkov, Z. (2011) Prevalence and correlates of bipolar spectrum disorder in the world mental health survey initiative. *Arch. Gen. Psychiatry*. **68**, 241–51
5. Wyatt, R. J., and Henter, I. (1995) An economic evaluation of manic-depressive illness--1991. *Soc. Psychiatry Psychiatr. Epidemiol.* **30**, 213–9
6. Das Gupta, R., and Guest, J. F. (2002) Annual cost of bipolar disorder to UK society. *Br. J. Psychiatry*. **180**, 227–33
7. CADE, J. F. J. (1949) Lithium salts in the treatment of psychotic excitement. *Med. J. Aust.* **2**, 349–52
8. Geddes, J. R., Burgess, S., Hawton, K., Jamison, K., and Goodwin, G. M. (2004) Long-term lithium therapy for bipolar disorder: systematic review and meta-analysis of randomized controlled trials. *Am. J. Psychiatry*. **161**, 217–222
9. Burgess, S., Geddes, J., Hawton, K., Townsend, E., Jamison, K., and Goodwin, G. (2001) Lithium for maintenance treatment of mood disorders. *Cochrane Database Syst. Rev.* 10.1002/14651858.CD003013
10. Cipriani, A., Pretty, H., Hawton, K., and Geddes, J. R. (2005) Lithium in the prevention of suicidal behavior and all-cause mortality in patients with mood disorders: a systematic review of randomized trials. *Am. J. Psychiatry*. **162**, 1805–1819
11. Cipriani, A., Hawton, K., Stockton, S., and Geddes, J. R. (2013) Lithium in the prevention of suicide in mood disorders: updated systematic review and meta-analysis. *BMJ*. **3646**, 1–13
12. Schou, M., Amdisen, A., and Trap-Jensen, J. (1968) Lithium poisoning. *Am. J. Psychiatry*. **125**, 520–7
13. Schou, M. (1984) Long-lasting neurological sequelae after lithium intoxication. *Acta Psychiatr. Scand.* **70**, 594–602
14. Adityanjee, Munshi, K. R., and Thampy, A. The syndrome of irreversible lithium-effectuated neurotoxicity. *Clin. Neuropharmacol.* **28**, 38–49
15. Lazarus, J. H. (2009) Lithium and thyroid. *Best Pract. Res. Clin. Endocrinol. Metab.* **23**, 723–33
16. Rej, S., Herrmann, N., and Shulman, K. (2012) The effects of lithium on renal function in older adults--a systematic review. *J. Geriatr. Psychiatry Neurol.* **25**, 51–61
17. Werneke, U., Ott, M., Renberg, E. S., Taylor, D., and Stegmayr, B. (2012) A decision analysis of long-term lithium treatment and the risk of renal failure. *Acta Psychiatr. Scand.* **126**, 186–97
18. McKnight, R. F., Adida, M., Budge, K., Stockton, S., Goodwin, G. M., and Geddes, J. R. (2012) Lithium toxicity profile: A systematic review and meta-analysis. *Lancet*. **379**, 721–728
19. Malhi, G. S., Tanious, M., Das, P., Coulston, C. M., and Berk, M. (2013) Potential

mechanisms of action of lithium in bipolar disorder: Current understanding. *CNS Drugs*. **27**, 135–153
20. Amari, L., Layden, B., Rong, Q., Geraldes, C. F., and Mota de Freitas, D. (1999) Comparison of fluorescence, (31)P NMR, and (7)Li NMR spectroscopic methods for investigating Li(+)/Mg(2+) competition for biomolecules. *Anal. Biochem.* **272**, 1–7
21. Mota de Freitas, D., Castro, M. M. C. a, and Geraldes, C. F. G. C. (2006) Is competition between Li+ and Mg2+ the underlying theme in the proposed mechanisms for the pharmacological action of lithium salts in bipolar disorder? *Acc. Chem. Res.* **39**, 283–91
22. Hallcher, L. M., and Sherman, W. R. (1980) The effects of lithium ion and other agents on the activity of myo-inositol-1-phosphatase from bovine brain. *J. Biol. Chem.* **255**, 10896–901
23. Ackermann, K. E., Gish, B. G., Honchar, M. P., and Sherman, W. R. (1987) Evidence that inositol 1-phosphate in brain of lithium-treated rats results mainly from phosphatidylinositol metabolism. *Biochem. J.* **242**, 517–24
24. Free, B. R., Hazelwood, L. A., Namkung, Y., Rankin, M. L., Rex, E. B., and Sibley, D. R. (2007) Chapter 3: Intracellular signaling. in *Contemporary Neuropharmacology*, 1st Ed. (Sibley, D. R., Hanin, I., Kuhar, M., and Sklonick, P. eds), pp. 81–87, John Wiley & Sons, New Jersey
25. Majerus, P. W. (1992) Inositol phosphate biochemistry. *Annu. Rev. Biochem.* **61**, 225–50
26. Gould, T. D., and Manji, H. K. (2002) Signaling networks in the pathophysiology and treatment of mood disorders. *J. Psychosom. Res.* **53**, 687–97
27. Gani, D., Downes, C. P., Batty, I., and Bramham, J. (1993) Lithium and myo-inositol homeostasis. *Biochim. Biophys. Acta*. **1177**, 253–69
28. Berridge, M. J., Downes, C. P., and Hanley, M. R. (1989) Neural and Developmental Actions of Lithium: A Unifying Hypothesis. *Cell*. 10.1016/0092-8674(89)90026-3
29. Atack, J. R., and Fletcher, S. R. (1994) Inhibitors of inositol monophosphatase. *Drugs Future*. 10.3109/14756369909036548
30. Atack, J. R., Prior, a M., Fletcher, S. R., Quirk, K., McKernan, R., and Ragan, C. I. (1994) Effects of L-690,488, a prodrug of the bisphosphonate inositol monophosphatase inhibitor L-690,330, on phosphatidylinositol cycle markers. *J. Pharmacol. Exp. Ther.* **270**, 70–6
31. Shtein, L., Toker, L., Bersudsky, Y., Belmaker, R., and Agam, G. (2013) The inositol monophosphatase inhibitor L-690,330 affects pilocarpine-behavior and the forced swim test. *Psychopharmacology (Berl).* **227**, 503–508
32. Baker, R., Kulagowski, J. J., Billington, D. C., Leeson, P. D., Lennon, I. C., and Liverton, N. (1989) Synthesis of 2- and 6-deoxyinositol 1-phosphate and the role of the adjacent hydroxy groups in the mechanism of inositol monophosphatase. *J. Chem. Soc. Chem. Commun.* 10.1039/c39890001383
33. Baker, R., Leeson, P. D., Liverton, N. J., and Kulagowski, J. J. (1990) Identification of (1S)-phosphoryloxy-(2R,4S)-dihydroxycyclohexane as a potent inhibitor of inositol monophosphatase. *J. Chem. Soc. Chem. Commun.* 10.1039/c39900000462
34. Atack, J. R., Cook, S. M., Watt, A. P., Fletcher, S. R., Ragan, C. I., L-, B., Atack, J. R., Cook, S. M., Watt, A. P., Fletcher, S. R., and Ragan, C. I. (1993) In vitro and in vivo inhibition of inositol monophosphatase by the bisphosphonate L-690,330. *J. Neurochem.* **60**, 652–8
35. Niesen, F. H., Berglund, H., and Vedadi, M. (2007) The use of differential scanning fluorimetry to detect ligand interactions that promote protein stability. *Nat. Protoc.* **2**, 2212–

2221
36. McAllister, G., Whiting, P., Hammond, E. A., Knowles, M. R., Atack, J. R., Bailey, F. J., Maigetter, R., and Ragan, C. I. (1992) cDNA cloning of human and rat brain myo-inositol monophosphatase. Expression and characterization of the human recombinant enzyme. *Biochem. J.* **284 (Pt 3**, 749–754
37. Bone, R., Springer, J. P., and Atack, J. R. (1992) Structure of inositol monophosphatase, the putative target of lithium therapy. *Proc. Natl. Acad. Sci. U. S. A.* **89**, 10031–5
38. Singh, N., Halliday, A. C., Knight, M., Lack, N. a, Lowe, E., and Churchill, G. C. (2012) Cloning, expression, purification, crystallization and X-ray analysis of inositol monophosphatase from Mus musculus and Homo sapiens. *Acta Crystallogr. Sect. F. Struct. Biol. Cryst. Commun.* **68**, 1149–52
39. Bone, R., Frank, L., Springer, J. P., and Atack, J. R. (1994) Structural studies of metal-binding by inositol monophosphatase - evidence for 2-metal ion catalysis. *Biochemistry*. **33**, 9468–9476
40. Gee, N. S., Ragan, C. I., Watling, K. J., Aspley, S., Jackson, R. G., Reid, G. G., Gani, D., and Shute, J. K. (1988) The purification and properties of myo-inositol monophosphatase from bovine brain. *Biochem. J.* **249**, 883–889
41. Attwood, P. V, Ducep, J. B., and Chanal, M. C. (1988) Purification and properties of myo-inositol-1-phosphatase from bovine brain. *Biochem. J.* **253**, 387–394
42. Takimoto, K., Okada, M., Matsuda, Y., and Nakagawa, H. (1985) Purification and properties of myo-inositol-1-phosphatase from rat brain. *J. Biochem.* **98**, 363–370
43. Parthasarathy, R., Parthasarathy, L., and Vadnal, R. (1997) Brain inositol monophosphatase identified as a galactose 1-phosphatase. *Brain Res.* **778**, 99–106
44. Ganzhorn, A. J., Lepage, P., Pelton, P. D., Strasser, F., Vincendon, P., and Rondeau, J. M. (1996) The contribution of lysine-36 to catalysis by human myo-inositol monophosphatase. *Biochemistry*. **35**, 10957–10966
45. Stieglitz, K. A., Johnson, K. A., Yang, H., Roberts, M. F., Seaton, B. A., Head, J. F., and Stec, B. (2002) Crystal structure of a dual activity IMPase/FBPase (AF2372) from Archaeoglobus fulgidus. The story of a mobile loop. *J. Biol. Chem.* **277**, 22863–22874
46. Bone, R., Frank, L., Springer, J. P., Pollack, S. J., Osborne, S. A., Atack, J. R., Knowles, M. R., McAllister, G., Ragan, C. I., and Broughton, H. B. (1994) Structural analysis of inositol monophosphatase complexes with substrates. *Biochemistry*. **33**, 9460–7
47. Ganzhorn, A. J., and Rondeau, J. M. (1997) Structure of an Enzyme-Substrate Complex and the Catalytic Mechanism of Human Brain Myo-Inositol Monophosphatase. *Protein Eng. Des. Sel.* **10**, 61–70
48. D'Angelo, E., Crutchfield, J., and Vandiviere, M. Rapid, sensitive, microscale determination of phosphate in water and soil. *J. Environ. Qual.* **30**, 2206–2209
49. O'Toole, M., Lau, K. T., Shepherd, R., Slater, C., and Diamond, D. (2007) Determination of phosphate using a highly sensitive paired emitter-detector diode photometric flow detector. *Anal. Chim. Acta*. **597**, 290–294
50. Itaya, K., and Ui, M. (1966) A new micromethod for the colorimetric determination of inorganic phosphate. *Clin. Chim. Acta.* **14**, 361–366
51. Winn, M. D., Ballard, C. C., Cowtan, K. D., Dodson, E. J., Emsley, P., Evans, P. R., Keegan, R. M., Krissinel, E. B., Leslie, A. G. W., McCoy, A., McNicholas, S. J., Murshudov, G. N., Pannu, N. S., Potterton, E. A., Powell, H. R., Read, R. J., Vagin, A., and Wilson, K. S. (2011) Overview of the CCP4 suite and current developments. *Acta Crystallogr. Sect. D*

Biol. Crystallogr. **67**, 235–242
52. Adams, P. D., Afonine, P. V., Bunkóczi, G., Chen, V. B., Davis, I. W., Echols, N., Headd, J. J., Hung, L. W., Kapral, G. J., Grosse-Kunstleve, R. W., McCoy, A. J., Moriarty, N. W., Oeffner, R., Read, R. J., Richardson, D. C., Richardson, J. S., Terwilliger, T. C., and Zwart, P. H. (2010) PHENIX: A comprehensive Python-based system for macromolecular structure solution. *Acta Crystallogr. Sect. D Biol. Crystallogr.* **66**, 213–221
53. Bricogne, G., Blanc, E., Brandl, M., Flensburg, C., Keller, P., Paciorek, W., Roversi, P., Sharff, A., Smart, O. S., Vonrhein, C., and Womack, T. O. (2011) Buster
54. Emsley, P., Lohkamp, B., Scott, W. G., and Cowtan, K. (2010) Features and development of Coot. *Acta Crystallogr. Sect. D Biol. Crystallogr.* **66**, 486–501

FOOTNOTES

This work was supported in whole or part by XXXXX grants.

The abbreviations used are: DAG, diacylglycerol; DSF, differential scanning fluorimetry; IC_{50}, inhibitory concentration; IMPase, inositol monophosphatase; Ins1P, inositol 1-phophsphate; IP_3, Inositol 1,4,5-trisphosphate; PI, Phosphoinositide/phosphatidylinositol; PIP, Phosphatidylinositol phosphate; PIP_2, Phosphatidylinositol 4,5-bisphosphate; PLC, Phospholipase C; RMSD, Root-mean-square deviation of atomic positions.

FIGURE LEGENDS

FIGURE 1. Dose response of L-690,330 in the malachite green and DSF assay. *A*, dose dependent effect of L-690,330 on IMPase melting point is shown. L-690,330 stabilizes IMPase and increases melting point in a concentration dependent fashion. Data is expressed as the mean of two independent experiments and standard deviation is represented by the filled area or error bars. *B*, dose response of L-690,330 in the malachite green assay. An IC_{50} of 0.22 ± 0.01 µM (n= 3) was determined. Data is expressed as mean of three independent experiments; standard deviation is represented by the error bars

FIGURE 2. Active site of IMPase co-crystallized with manganese and MES. MES exclusively interacts with the three manganese ions (Mn1, Mn2 and Mn3) via its sulfonic moiety and no interaction to other pocket residues is seen.

FIGURE 3. Comparison of chain A and chain B of IMPase crystallized in the presence of calcium and Ins1P. Electron density for all residues is seen in chain A while residues 28-43 and 73-78 in chain B could not be resolved and missing residues are indicated by the dotted line.

FIGURE 4. Mobile loop. *A*, the loop comprised of residues 28-43 is directed towards the active site in the crystal structure of IMPase crystallized in the presence of manganese and MES. Lys36 points inwards and forms a salt bridge with Glu71, as well as a hydrogen bond with a conserved water that is coordinated to the third manganese Mn3. *B*, this same mobile loop takes in an outwards pointing conformation in the structure co-crystallized with calcium and Ins1P. Lys36 points away and does not form part of the pocket.

FIGURE 5. Active site of IMPase co-crystallized with calcium and Ins1P. *A*, key interactions of Ins1P with IMPase are the metal coordinating bonds to the phosphoryl group and the hydrogen bond of the inositol ring to Glu213, as well as hydrogen bonds to backbone residues Gly96 to Thr96. *B*, superimposition of both resolved crystal structure is shown. The manganese and calcium metal ions coordinate identically in the active site of both structures. A glycerol found in the structure with manganese takes in the space of the inositol ring and forms identical hydrogen bonds to Ala196 and Glu213.

FIGURE 6. L-690,330 in the active site of IMPase. L-690,330 takes in identical orientation as the substrate. The bisphosphonate group rigorously forms metal bonds with all manganese ions (Mn1, Mn2 and Mn3), as well as additional hydrogen bonds to backbone residues Trp219 and Asp220 that are not observed with the substrate Ins1P.

FIGURE 1.

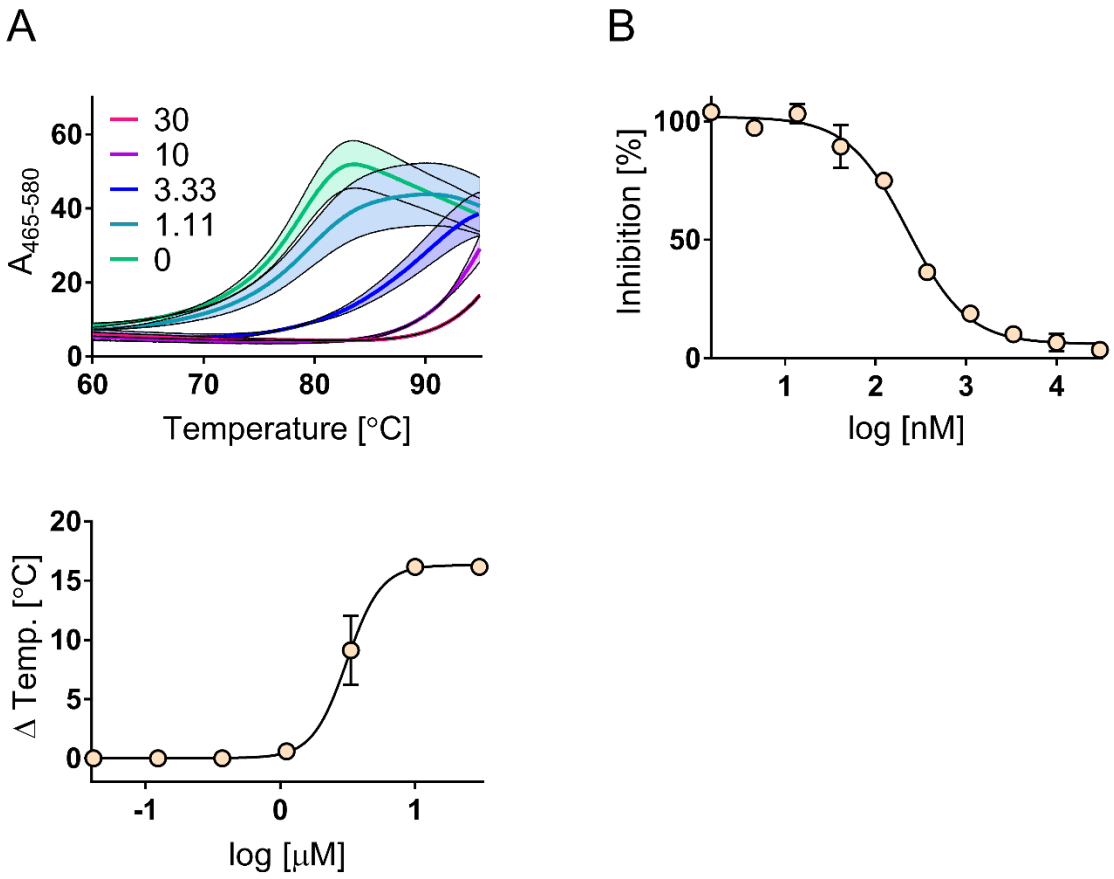
A
B
30
10
3.33
1.11
0
$A_{465-580}$
Temperature [°C]
Inhibition [%]
log [nM]
Δ Temp. [°C]
log [μM]

FIGURE 2.

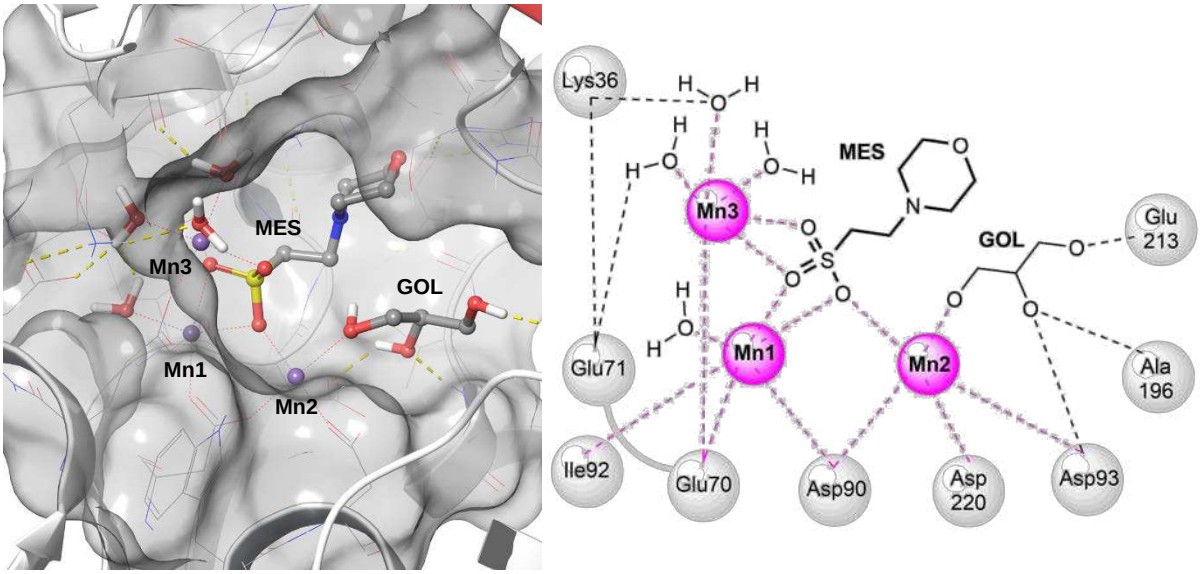
MES
Mn3
GOL
Mn1
Mn2
Lys36
MES
Mn3
GOL
Glu
213
Mn1
Mn2
Glu71
Ala
196
Ile92
Glu70
Asp90
Asp
220
Asp93

FIGURE 3.

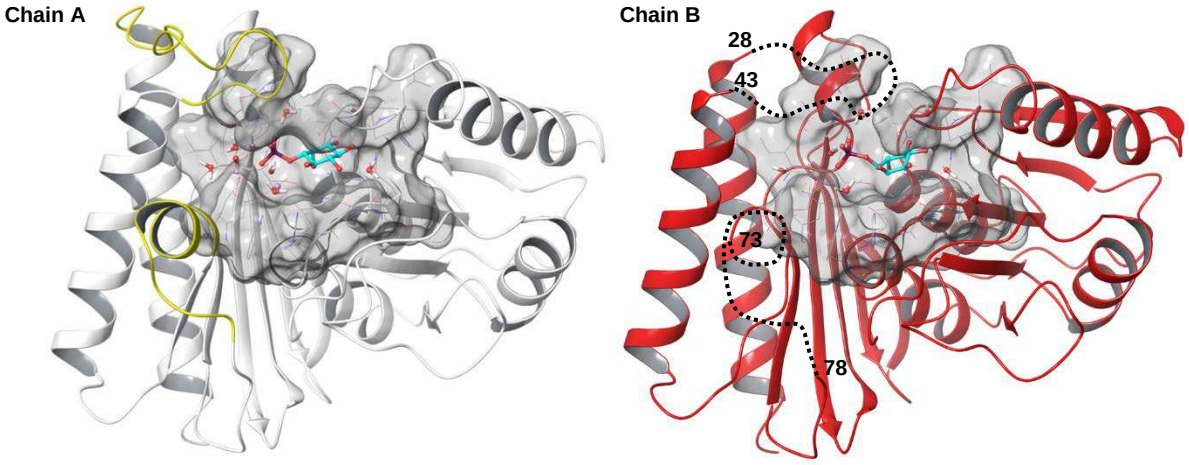

FIGURE 4.

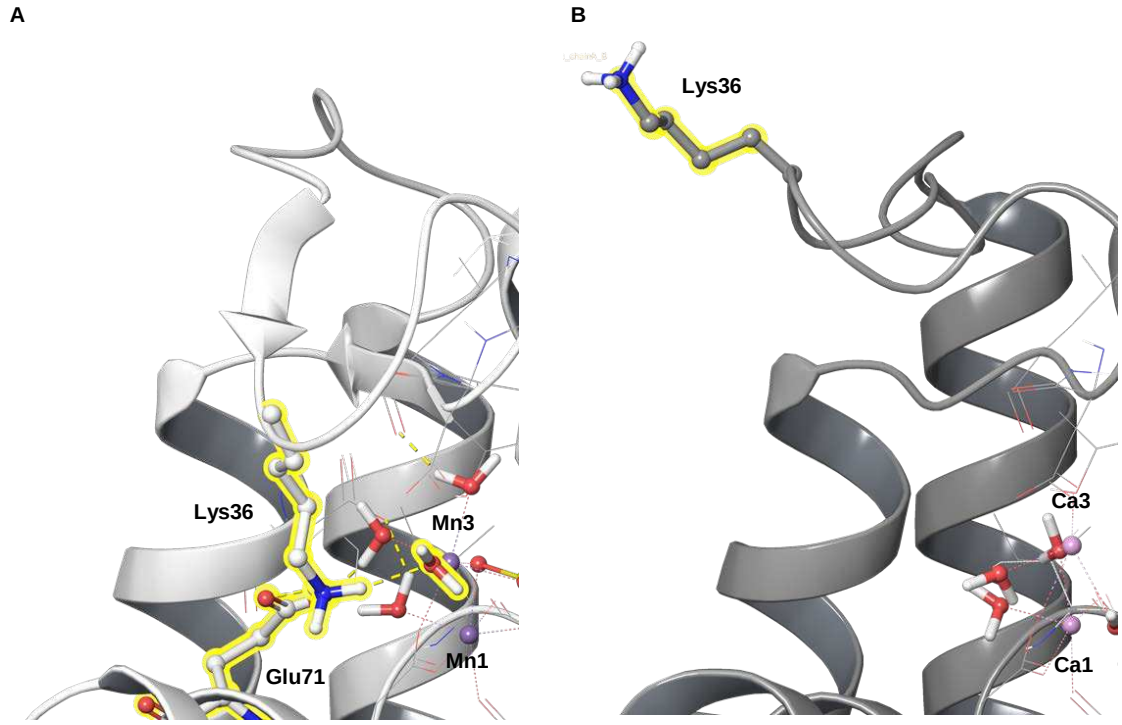

FIGURE 5.

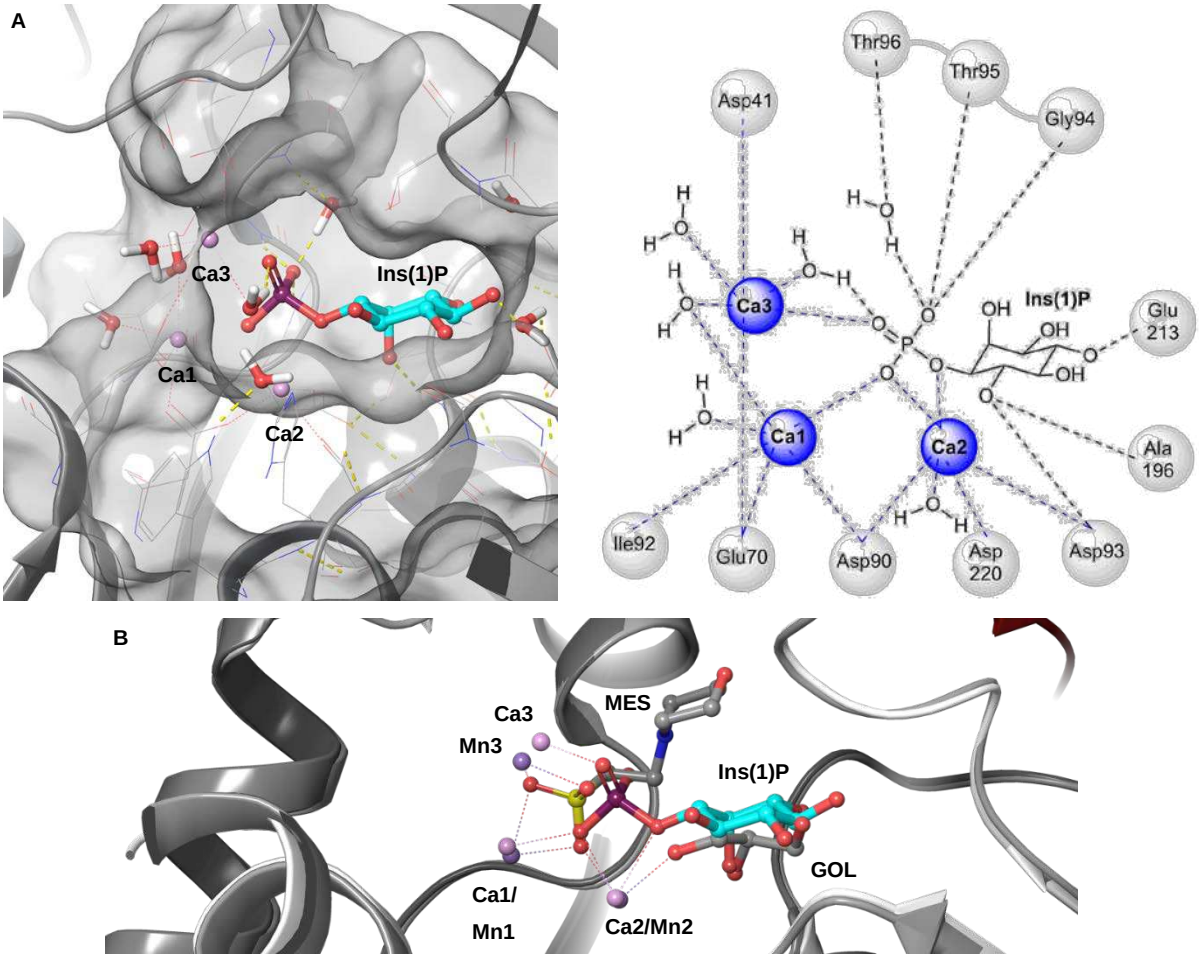
A
Ca3
Ins(1)P
Ca1
Ca2
Thr96
Thr95
Asp41
Gly94
Ins(1)P
Glu 213
Ca3
Ca1
Ca2
Ala 196
Ile92
Glu70
Asp90
Asp 220
Asp93
B
Ca3
Mn3
MES
Ins(1)P
GOL
Ca1/
Mn1
Ca2/Mn2

FIGURE 6.

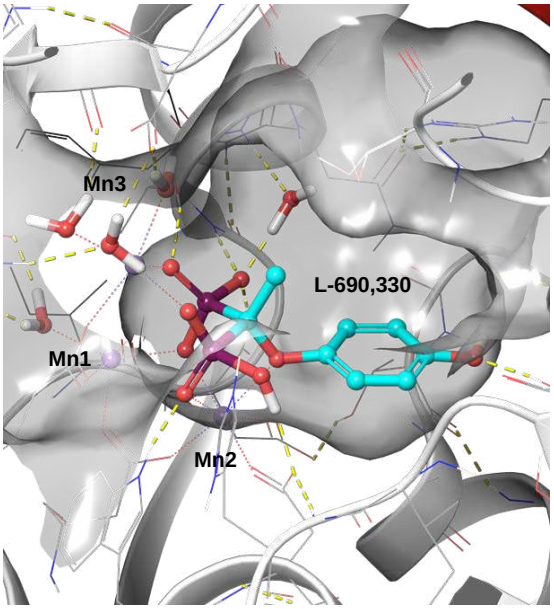
Mn3
L-690,330
Mn1
Mn2

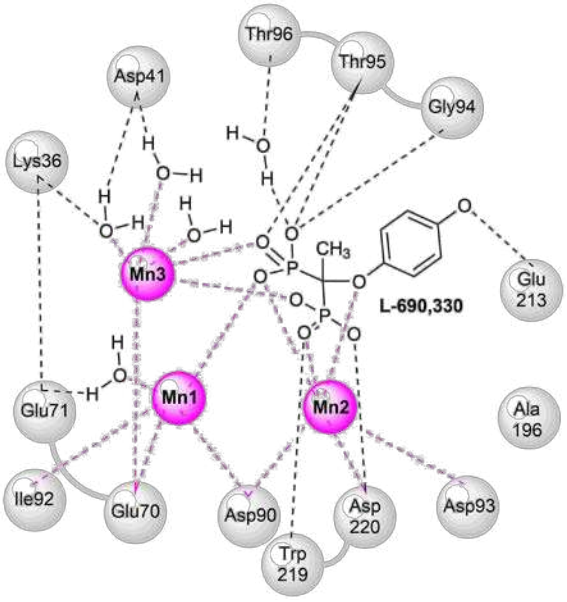
Thr96
Thr95
Asp41
Gly94
Lys36
Mn3
L-690,330
Glu 213
Mn1
Mn2
Glu71
Ala 196
Ile92
Glu70
Asp90
Asp 220
Asp93
Trp 219

TABLE 1.

	IMPase with manganese and MES	IMPase with calcium and Ins1P	IMPase with manganese and L-690,330
Wavelength (Å)	0.9795	0.9141	0.9141
Resolution range (Å)	42.47 - 1.73 (1.792 - 1.73)	20.21 - 1.68 (1.74 - 1.68)	20.35 - 1.39 (1.44 - 1.39)
Space group	P $3_2$21	P 1	P $3_2$21
Unit cell: a, b, c (Å)	84.94, 84.94, 152.51	56.92, 61.57, 76.3	85.29, 85.29, 151.51
	90, 90, 120	87, 87.17, 80.34	90, 90, 120
Total reflections	132014 (12971)	294100 (29110)	654228 (63759)
Unique reflections	67052 (6585)	112520 (11159)	128391 (12704)
Multiplicity	2.0 (2.0)	2.6 (2.6)	5.1 (5.0)
Completeness (%)	99.88 (99.91)	96.90 (95.63)	99.88 (99.90)
Mean I/sigma(I)	17.57 (2.34)	8.73 (2.11)	12.13 (2.43)
Wilson B-factor	21.55	20.30	12.35
R-merge	0.03154 (0.3805)	0.06425 (0.3999)	0.07519 (0.5912)
R-meas	0.04461	0.08021	0.08399
CC1/2	0.999 (0.7)	0.995 (0.828)	0.998 (0.782)
CC*	1 (0.908)	0.999 (0.952)	0.999 (0.937)
R-work	0.1712 (0.2863)	0.2160 (0.2896)	0.1459 (0.2335)
R-free	0.2100 (0.3030)	0.2501 (0.3252)	0.1647 (0.2456)
Number of non-hydrogen atoms	4797	8256	5141
macromolecules	4222	7802	4307
ligands	66	97	157
water	509	357	677
Protein residues	548	1049	550
RMS(bonds)	0.007	0.007	0.015
RMS(angles)	1.12	1.11	1.72
Ramachandran favored (%)	98	98	98
Ramachandran outliers (%)	0	0.38	0
Clashscore	6.69	4.72	3.90
Average B-factor	25.80	26.90	19.60
macromolecules	24.40	26.70	16.90
ligands	31.80	30.90	26.80
solvent	36.00	30.90	35.30